Original Article

Mangostanaxanthone VIIII, a new xanthone from *Garcinia mangostana* pericarps, α-amylase inhibitory activity, and molecular docking studies

Sabrin R.M. Ibrahim [a,b,*], Gamal A. Mohamed [c,d], Maan T. Khayat [e], Sahar Ahmed [a,f], Hany Abo-Haded [g], Khalid Z. Alshali [h]

[a] Department of Pharmacognosy and Pharmaceutical Chemistry, College of Pharmacy, Taibah University, Al Madinah Al Munawwarah, Saudi Arabia
[b] Department of Pharmacognosy, Faculty of Pharmacy, Assiut University, Assiut, Egypt
[c] Department of Natural Products and Alternative Medicine, Faculty of Pharmacy, King Abdulaziz University, Jeddah, Saudi Arabia
[d] Department of Pharmacognosy, Faculty of Pharmacy, Al-Azhar University, Assiut, Egypt
[e] Department of Pharmaceutical Chemistry, Faculty of Pharmacy, King Abdulaziz University, Jeddah, Saudi Arabia
[f] Department of Medicinal Chemistry, Faculty of Pharmacy, Assiut University, Assuit, Egypt
[g] Cardiology Unit, College of Medicine, Taibah University, Al Madinah Al Munawwarah, Saudi Arabia
[h] Department of Medicine, Faculty of Medicine, King Abdulaziz University, Jeddah, Saudi Arabia

ARTICLE INFO

ABSTRACT

A new xanthone: mangostanaxanthone VIIII [1,3,5,6,7-pentahydroxy-2-(3-methylbut-2-enyl)-8-(3-hydroxy-3-methylbut-1-enyl) xanthone] (**5**) and four known xanthones: mangostanaxanthones I (**1**) and II (**2**), γ-mangostin (**3**), and mangostanaxanthone VII (**4**) were separated and characterized from the acetone fraction of *Garcinia mangostana* L., Clusiaceae (mangosteen) pericarps. Their structures were established based on various spectroscopic analyses in addition to HRMS and comparison with the literature. The α-amylase inhibitory potential of the isolated metabolites was evaluated. Compounds **1**, **2**, and **5** had the highest activity with % inhibition 72.5, 86.5, and 81.8, respectively compared to acarbose (97.1%, reference α-amylase inhibitor). The molecular docking study of the tested metabolites was estimated to shade up the rational explanation of the α-amylase inhibitory activity results. Moreover, the pharmacokinetic parameters were assessed using Swiss ADME. It is noteworthy that **1**, **2**, and **5** had similar binding poses as the X-ray crystal structure of acarbose, whereas the other metabolites possessed different binding mode that decreased their inhibitory capacity. Thus, these data reinforced the health benefit of mangosteen as an alternative medicine to help lowering the postprandial glucose absorption. Therefore, it could have a good potential for the treatment of diabetes.

Introduction

Diabetes is continuing to be a major health problem worldwide. It is characterized by a deficiency in insulin action and/or insulin secretion accompanied by hyperglycemia and disturbance in protein, lipid, and carbohydrate metabolism (Rahimi et al., 2005; Mata et al., 2013). The α-amylase enzyme plays a significant role in the digestion of starch, where it hydrolyzes starch producing low molecular weight sugars and dextrins (Sales et al., 2012). Its inhibition will retard the carbohydrates digestion and decrease the glucose absorption rate consequently reduces the post-prandial blood glucose level that is a valuable strategy in treating type-2 diabetes (Jayaraj et al., 2013). Also, this helps in the treatment of obesity (Tucci et al., 2010). Acarbose and miglitol are well-known α-amylase inhibitors, which have been widely used for treating diabetes (Barrett and Udani, 2011). However, they have side effects such as abdominal pain, diarrhea, and flatulence (Gyémánt et al., 2003; Rosas-Ramírez et al., 2018). Therefore, the search for the safe and effective hypoglycemic agents continues to be an important goal for various researches. Medicinal plants are a wealthy pool of constituents with a potential α-amylase inhibitory effect, particularly the phenolic constituents and can be utilized as functional or therapeutic food sources (Sales et al., 2012). *Garcinia mangostana* L., Clusiaceae (mangosteen, mangkhut, queen

of fruits) is commonly consumed in the Southeast Asian countries due to its pleasant aroma, unique sweet taste, and high nutritional value (Mohamed et al., 2014, 2017). It has been used in various traditional medicines for treating different ailments such as hyperkeratosis, menstrual disorders, gleet, cystitis, psoriasis, wounds, skin infections, gonorrhea, amoebic dysentery, inflammation, diarrhea, and ulcers (Abdallah et al., 2016a,b,c, 2017; Mohamed et al., 2014, 2017; Ibrahim et al., 2018a,b,c,d). It is considered to be a wealthy pool of phenolics and oxygenated and prenylated xanthones, which possessed a wide variety of bioactivities (Abdallah et al., 2016a,b,c, 2017; Ibrahim et al., 2018a,b,c,d). In continuing of our effort to discover structurally unique biometabolites from *G. mangostana*, its acetone fraction was subjected to a phytochemical study leading to the separation and structural characterization of a new xanthone, mangostanaxanthone VIIII (**5**), together with four known xanthones (**1–4**). Their structures were verified by one- and two-dimensional NMR analyses as well as comparison with the data for the related known compounds. Moreover, the α-amylase inhibitory potential of the isolated metabolites was evaluated and the molecular modeling study of the tested metabolites was performed.

Materials and methods

General experimental procedures

UV spectra were recorded in MeOH on a Shimadzu 1601 UV/VIS spectrophotometer (Shimadzu, Kyoto, Japan). The IR spectrum was measured on a Shimadzu Infrared-400 spectrophotometer (Shimadzu, Kyoto, Japan). A LCQ DECA mass spectrometer (ThermoFinnigan, Bremen, Germany) was utilized to measure ESIMS. HRESIMS was carried out by LTQ-Orbitrap spectrometer (ThermoFinnigan, Bremen, Germany). NMR spectra were recorded on Bruker Avance DRX 400 MHz spectrometers (Bruker BioSpin, Billerica, MA, USA). Sephadex LH-20 (0.25–0.1 mm, Pharmacia Fine Chemical Co. Ltd, Piscataway, NJ), RP-18 (0.04–0.063 mm), and silica gel 60 (0.04–0.063 mm, Merck, Darmstadt, Germany) were used for column chromatography. Pre-coated silica gel plates Kieselgel 60 F_{254} (0.25 mm, Merck, Darmstadt, Germany) were used for thin-layer chromatographic (TLC) analysis. The compounds were detected by UV absorption at λ_{max} 255 and 366 nm followed by spraying with a *p*-anisaldehyde:H_2SO_4 spray reagent, then heating at 110 °C for 1–2 min. All chemicals materials were secured by Sigma Chemical Aldrich (St. Louis, MO, USA).

Plant material

Garcinia mangostana L., Clusiaceae, fruits were bought in August 2016 from a local market in Saudi Arabia. Its authentication was carried out as previously stated (Ibrahim et al., 2018a,b,c,d; Mohamed et al., 2017).

Extraction and isolation

The air-dried powdered pericarps of *G. mangostana* (100 g) were extracted with acetone (6× 3 l) at room temperature. The acetone extract was evaporated and concentrated under reduced pressure to afford a dark brown residue (4.1 g). The extract (4.1 g) was chromatographed over a silica gel (SiO₂) column (350 g × 100 × 3 cm) using hexane:EtOAc gradient to obtain five fractions: GM-1 to GM-5. Fraction GM-2 (752 mg; hexane:EtOAc, 75:25) was

Table 1
NMR spectral data of compound **5** (CD₃OD, 400 and 100 MHz).

No.	δ_H (J (Hz))	δ_C	HMBC
1	–	159.4 (C)	–
2	–	111.4 (C)	–
3	–	162.4 (C)	–
4	6.32 s	93.2 (CH)	2, 3, 4a, 8b
4a	–	152.1 (C)	–
4b	–	138.5 (C)	–
5	–	136.8 (C)	–
6	–	140.8 (C)	–
7	–	144.0 (C)	–
8	–	118.7 (C)	–
8a	–	113.8 (C)	–
8b	–	103.8 (C)	–
9	–	183.9 (C)	–
1′	3.34[a]	23.7 (CH₂)	1, 2, 3, 2′
2′	5.24 brt (7.0)	124.0 (CH)	2, 4′, 5′
3′	–	132.6 (C)	–
4′	1.66 brs	26.0 (CH₃)	2′, 3′, 5′
5′	1.78 brs	18.2 (CH₃)	2′, 3′, 4′
1″	7.99 d (10.0)	122.6 (CH)	7, 8, 8a, 3″
2″	5.79 d (10.0)	131.7 (CH)	3″, 4″, 5″
3″	–	77.0 (C)	–
4″	1.47 s	27.2 (CH₃)	2″, 3″, 5″
5″	1.47 s	27.2 (CH₃)	2″, 3″, 4″

[a] Under-solvent.

chromatographed on SiO₂ column (60 g × 50 × 2 cm) and eluted with hexane:EtOAc (97:3 to 85:15) to get impure **1** and **2**. Their purification were performed using RP-18 (50 g × 50 × 2 cm) column eluting with MeOH:H₂O gradient to give **1** (11.3 mg) and **2** (6.9 mg). SiO₂ column (100 g × 50 × 3 cm) of fraction GM-3 (981 mg; hexane:EtOAc, 50:50) using hexane:EtOAc (95:5 to 80:20) gave two major spots. Similarly, the separation of the two major spots was done as in fraction GM-2 to get **3** (14.2 mg) and **4** (9.4 mg). Fraction GM-4 (817 mg; hexane:EtOAc, 25:75) was chromatographed over a sephadex LH-20 column (50 g × 50 × 2 cm) using MeOH:CHCl₃ (90:10) as an eluent to obtain impure **5**, which was purified on SiO₂ column (50 g × 50 × 2 cm) using hexane:EtOAc gradient to yield **5** (4.6 mg).

Spectroscopic data

Mangostanaxanthone VIIII [1,3,5,6,7-pentahydroxy-2-(3-methylbut-2-enyl)-8-(3-hydroxy-3-methylbut-1-enyl) xanthone] (5)

Yellow amorphous powder; UV (MeOH) λ_{max} (log ε): 247 (4.49), 280 (4.47), 320 (4.15), 369 (3.73) nm; IR (KBr) ν_{max}: 3425, 2859, 1650, 1625, 1612, 1543, 892 cm⁻¹; NMR spectroscopic data, see Table 1; HRESIMS *m/z*: 429.1554 [M+H]⁺ (calcd for 429.1549, $C_{23}H_{25}O_8$).

α-Amylase inhibitory activity

The assay was carried out using EnzCheck® Ultra Amylase Assay Kit (E33651) as previously outlined (Ibrahim et al., 2015, 2017a,b; Mohamed and Alliuocide, 2008).

Molecular modeling

The modeling experiments were performed using SYBYL_X software (Tripos, St. Louis) versions 2.0 or 2.0_64 as previously outlined (Ibrahim et al., 2018e). The α-amylase crystal structure was downloaded from the Brookhaven website (www.rcsb.org) (PDB:1OSE).

The binding modes of the docked ligands were evaluated and compared to the co-crystallized ligand to identify the possible differences and similarities. Maestro academic software was used to generate 3D and 2D figures.

## Results and discussion

Purification of the metabolites

The dried pericarps were extracted with acetone. The acetone extract was repeatedly separated on the SiO$_2$, RP-18, and Sephadex LH-20 columns to afford one new (**5**) and four known compounds (**1–4**).

Structural characterization of the isolated metabolites

Compound **5** was separated as a yellow amorphous powder. Its HRESIMS spectrum showed a protonated molecule at m/z 429.1554 [M+H]$^+$ (calcd for 429.1549, C$_{23}$H$_{25}$O$_8$) compatible with the molecular formula C$_{23}$H$_{24}$O$_8$, requiring 12 double bond equivalent (DBE). A fragment ion peak at m/z 412.1515 [M−H$_2$O]$^+$ (calcd for 412.1522, C$_{23}$H$_{24}$O$_7$) was observed in the HRESIMS spectrum. Compound **5** was 16 mass units more than mangostanaxanthone VII (**4**), indicating the presence of an additional hydroxyl group in **5**. It exhibited UV absorptions at λ_{max} 247, 280, 320, and 369 nm, suggesting an oxygenated xanthone framework of **5** (Xu et al., 2014; Ibrahim et al., 2018a,b,c). Its IR spectrum revealed bands for phenolic OH (3425 cm^{-1}) and chelated carbonyl (1650 cm^{-1}) (Xu et al., 2014; Ibrahim et al., 2018a,b,c). The IR, UV, and NMR data of **5** were similar to those of mangostanaxanthone VII (**4**), except the signals related to H-5/C-5 (δ_H 6.85/δ_C 103.3) were absent in **5**. The ^{13}C and HSQC spectra possessed 23 carbon resonances: 4 methines, 14 quaternary carbons, including an oxygen-bonded aliphatic carbon (δ_C 77.0, C-3″) and one carbonyl (δ_C 183.9, C-9), one methylene, and four methyls (Table 1). The aromatic proton signal at δ_H 6.32 in the ^{1}H spectrum, correlating to the carbon at δ_C 93.2 in the HSQC, was assigned to H-4/C-4. This was established by the observed HMBC correlations of H-4/C-3, C-2, C-4a, and C-8b. The signals for two methyls at δ_H 1.47 (H-4″, 5″)/δ_C 27.2 (C-4″, 5″), a di-substituted olefinic bond at δ_H 5.79 (H-2″)/131.7 (C-2″) and 7.99 (H-1″)/δ_C 122.6 (C-1″), and an oxygen-bonded quaternary carbon at δ_C 77.0 (C-3″) in ^{1}H and ^{13}C NMR indicated the presence of a 3-hydroxy-3-methylbut-1-enyl moiety in **5**. The HMBC correlations of H-2″/C-4″, C-3″, and C-5″, H-1″/C-3″, and H-5″ and H-4″/C-2″ and C-3″ proved the assignment of the 3-hydroxy-3-methylbut-1-enyl moiety (Mohamed et al., 2017). Its attachment at C-8 was secured by the HMBC correlations of H-1″/C-8a, C-8, and C-7. Moreover, the observed HSQC signals at δ_H 3.34 (H-1′)/δ_C 23.7 (C-1′), 5.24 (H-2′)/124.0 (C-2′), 132.6 (C-3′), 1.66 (H-4′)/26.0 (C-4′), and 1.78 (H-5′)/18.2 (C-5′) characterized the presence of for a 3-methylbut-2-enyl moiety (Ibrahim et al., 2018a,b,c,d). This was established by correlations of H-2′/C-5′ and C-4′, H-1′/C-2′ and C-3′, and H-4′ and H-5′ to C-2′ and C-3′ in the HMBC. Its attachment at C-2 was assured by the HMBC correlations of H-2′/C-2 and H-1′/C-1, C-2, and C-3. Therefore, **5** was identified as 1,3,5,6,7-pentahydroxy-2-(3-methylbut-2-enyl)-8-(3-hydroxy-3-methylbut-1-enyl) xanthone and named mangostanaxanthone VIIII.

The known metabolites: mangostanaxanthones I (**1**) (Mohamed et al., 2014), II (**2**) (Ghazali et al., 2010), γ-mangostin (**3**) (Ghazali et al., 2010), and mangostanaxanthone VII (**4**) (Ibrahim et al., 2018b) were assigned by comparing their spectroscopic data to the formerly published data.
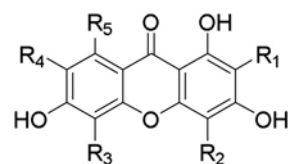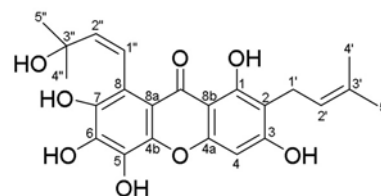

1 R$_1$=R$_3$=H; R$_2$=R$_5$=Gemyl; R$_4$=OCH$_3$
2 R$_1$=R$_2$=R$_5$=Prenyl; R$_3$=H; R$_4$=OCH$_3$
3 R$_1$=R$_5$=Prenyl; R$_2$=R$_3$=H; R$_4$=OH
4 R$_1$=Prenyl; R$_2$=R$_3$=H; R$_4$=OH; R$_5$=

5

α-Amylase inhibitory activity and molecular modeling study

The prevalence of diabetes is increasing all over the world; this indicates urgent needs for appropriate treatment. α-Amylase is a key enzyme in the digestive system and catalyzes the initial step in starch hydrolysis. Its inhibitors possess an important role in controlling diabetes. Medicinal plants and/or their constituents are drawing a lot of attention because of their demonstrated health benefits, with scientific evidence demonstrating that they possess a high number of protective biological properties, including antidiabetic, antioxidant, anti-inflammatory and other beneficial effects. They are considered convenient for the management of diabetes due to their traditional availability and acceptability, lesser side effects, and low costs. The previous report by Adnyana et al. (2016) stated that α-mangosteen and the pericarp extract of *G. mangostana* showed a concentration-dependent α-amylase inhibitory capacity (Adnyana et al., 2016). Moreover, Loo and Huang (2007) reported that the pericarp extract possessed inhibitory activity against α-amylase (Loo and Huang, 2007).

In this study, the α-amylase inhibitory capacity of the isolated metabolites was assessed. The results revealed that **1**, **2**, and **5** displayed the highest activity with % inhibition 72.5, 86.5, and 81.8, respectively compared to acarbose (97.1%, reference α-amylase inhibitor), while compounds **3** and **4** showed moderate activity (% inhibition 69.7 and 56.2, respectively) (Fig. 1).

The α-amylase enzyme crystal structure is composed of three structural domains: A, B, and C (Nahoum et al., 2000). The active site of the α-amylase is in domain A, which has a V-shaped
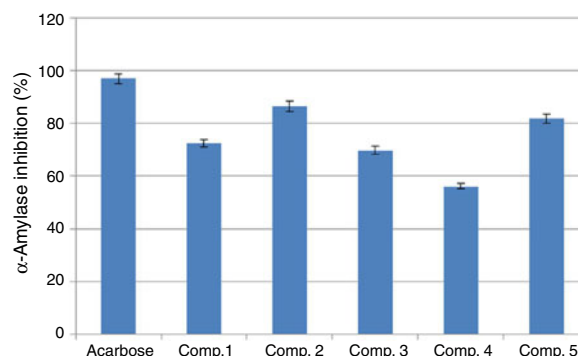

Fig. 1. α-Amylase inhibitory effects of xanthones **1–5** isolated from *Garcinia mangostana*.

Table 2
α-Amylase inhibitors predicted pharmacokinetic parameters and total score calculated by Surflex.

Compd No.	M. wt.	#Rotatable bonds	#H-bond acceptors	#H-bond donors	MR	TPSA	Log P	Log S	Lip. v	Total score
1	546.69	11	6	3	167.11	100.13	8.54	−9.06	1	8.32
2	464.56	6	6	4	139.24	111.13	6.29	−7.59	0	7.34
3	396.44	4	6	4	115.52	111.13	4.79	−6.14	0	6.96
4	412.43	4	7	5	117.51	131.36	3.95	−5.23	0	5.61
5	428.43	4	8	6	119.54	151.59	3.66	−5.09	1	7.55

M. wt., molecular weight; TPSA, polar surface area; Log P, calculated lipophilicity; Lip.V, number of violations of Lipinski rule.
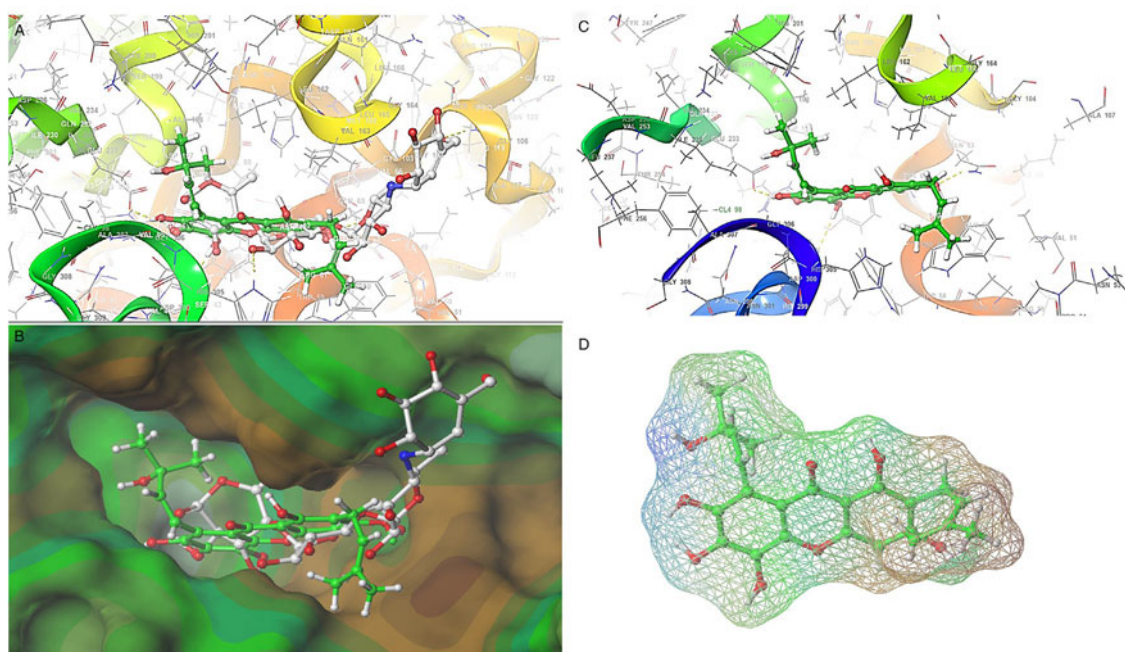

Fig. 2. (A) 3D model structure of **5** (green color) superimposed with acarbose (white color) in the active site of α-amylase. (B) **5** and acarbose in the catalytic site after surface generation. (C) 3D docked model of **1** in domain A illustrating H-bonds. (D) Extracted docked conformation of **5** by surflex in the active site.

depression (Nahoum et al., 2000). The selection of the porcine pancreatic α-amylase crystal structure 1OSE in this study was based on two main reasons. First, it forms a complex with acarbose which had been used as a reference standard. Second, the homology of the porcine and human pancreatic α-amylase is very similar (87.1%) compared with other amylases (Qian et al., 1997). In this work, the isolated xanthone derivatives were docked by Surflex then their poses were compared with those of acarbose. Moreover, using the web tool Swiss ADME (http://www.swissadme.ch), the pharmacokinetic parameters were estimated for all derivatives (Table 2). All derivatives shared the xanthone framework with some differences in the terminal side chains' lengths and positions. In contrast, these xanthones did not share any common structural features with acarbose. Thus, it is very important to study these analogs in 3D modeling with acarbose and shade up the rational explanation and correlation to the obtained inhibitory activity results.

From the crystal structure of acarbose, it was found that six hydrogen bonds (H-bond) were formed with the active site of the enzyme. Also, it is completely bound to the V-shaped pocket and this explained its complete inhibition of this enzyme among the other tested compounds. Interestingly, **5** shared the same binding region with a similar pose to acarbose (Fig. 2). However, **5** formed five H-bonds, including one H-bond with Gly-63, His-299, and Arg-195, and two H-bonds with Glu-233 (Fig. 4A). Moreover, the side chains at positions 2 and 8 of **5** showed Van der Waals interactions with Trp-58, Trp-59, and Val163 and Leu-163 and Ile-235, respectively. According to the 3D modeling, the terminal hydroxyl group at C-3" did not form any H-bond. Moreover, pi-pi stacking

interactions were observed between rings A and B of **5** with His-305 and His-101, respectively (Fig. 3A). The 3D modeling revealed the involvement of **1** with different interactions with the active site. For instance, rings A and B of **1** had pi-pi interactions with His-305, His-299, and Tyr-62 residues. The phenolic hydroxyl group at position 3 possessed three H-bonds with Arg-195, Glu-233, and Asp-197. In addition, the geranyl chain at position 4 exhibited hydrophobic interactions with Leu-162, Ile-235, and Lys-200, whereas the geranyl moiety at C-8 interacted with AA Val-163, Pro-54, Trp-58, and Trp-59 (Fig. 3B). Thus, it could be concluded that **1** was the highest scoring among other series (Table 2). Analog **2** which had three aliphatic chains at C-2, C-4, and C-8 showed moderate scoring and good inhibitory activity. This could be suggested by three major interactions which included three H-bonds with His-299, Asp-197, and Arg-195, a pi-pi stacking between ring A and His-305, and hydrophobic interactions between C-2, C-4, and C-8 prenyl side chains and Tyr-62, Trp-59, and Ala-198, respectively (Fig. 3C). Compound **4** which is structurally related to **5** but lacked a phenolic hydroxyl group at C-5 in ring B. This small difference had completely changed the binding interactions and resulted in different poses than **5** and acarbose. However, **4** formed two H-bonds with Lys-200 and His-201 (Fig. 4B). Moreover, pi-pi stacking interactions were illustrated between rings A and B and His-201 and Tyr-151, respectively (Fig. 4B). Accordingly, this could explain its lower inhibitory activity and scoring value compared to the other tested analogs. On the other hand, **3** which lacked the HO group at C-3″ that found in **4** and **5**, possessed three H-bonds with His-101, Ile-235, and Lys-200 as well as pi-pi interactions with His-201
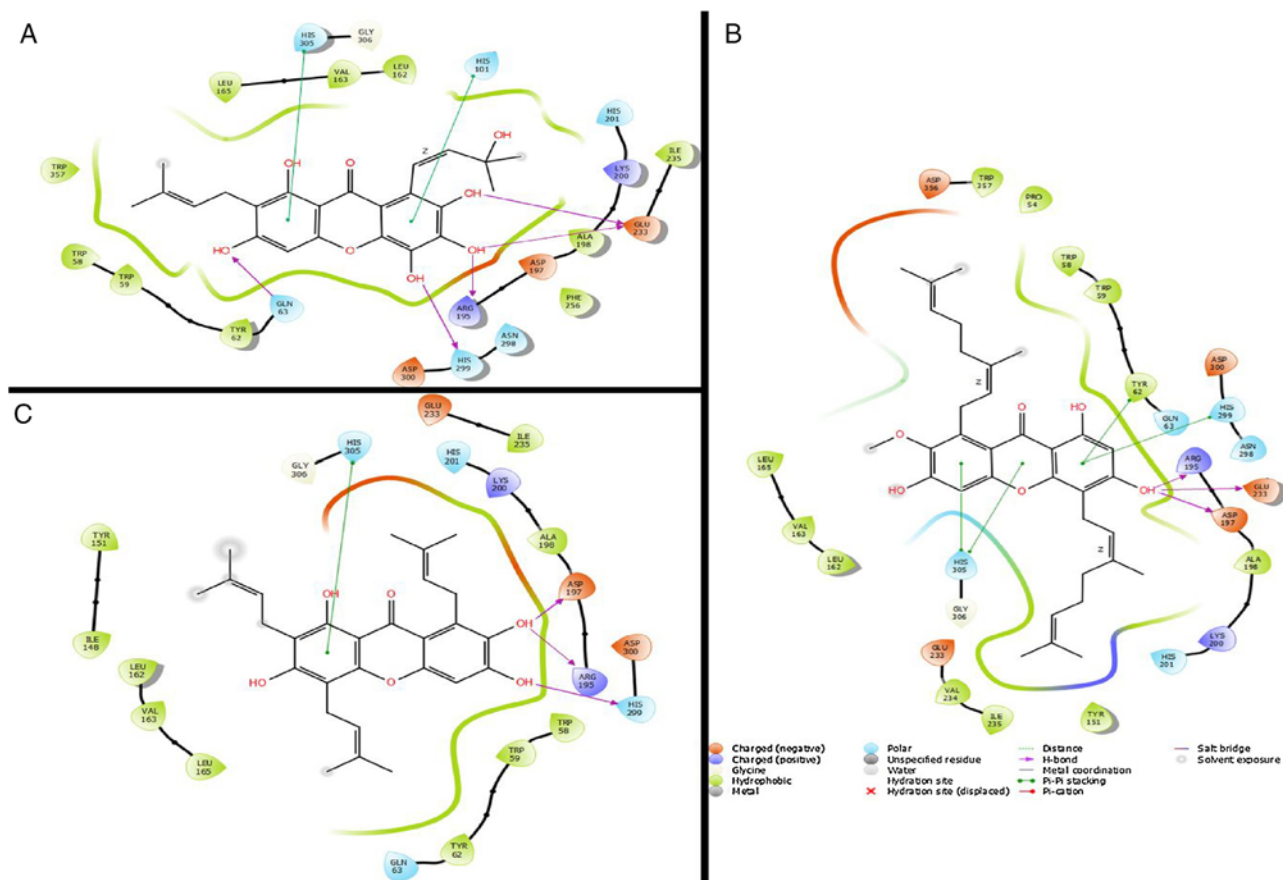
Fig. 3. 2D diagram of α-amylase inhibitors binding mode with amino acids residues involved in the interactions (A) **5**, (B) **1**, and (C) **2**.
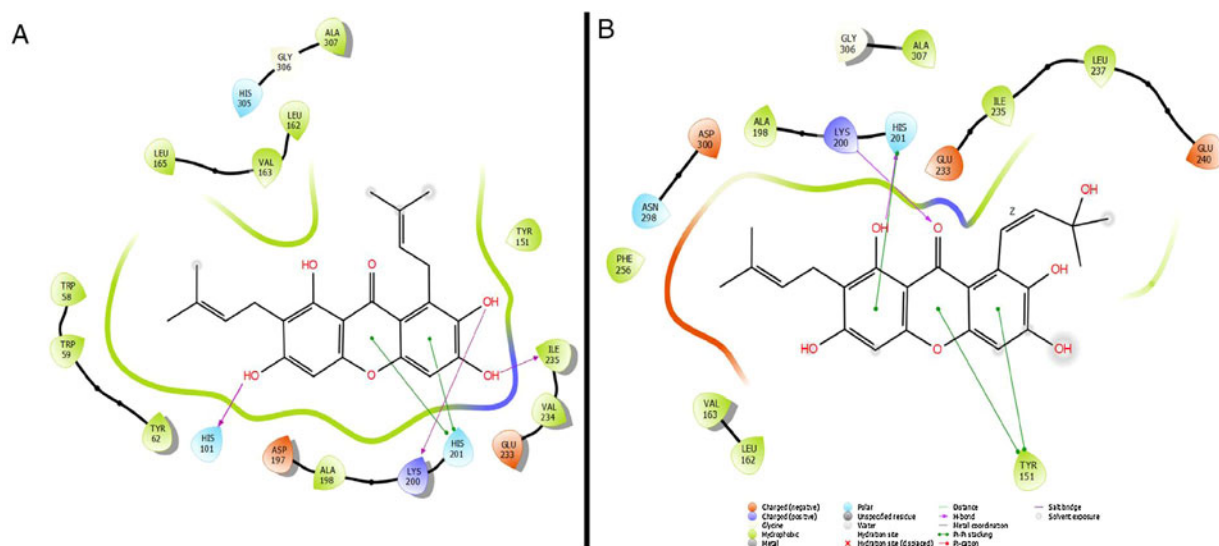

Fig. 4. 2D illustration interaction of **3** (A) and **4** (B) with α-amylase active site.

(Fig. 4A). The modeling results also illustrated that **3** had different binding mode compared to **5** and acarbose, which provided the reason for the decrease in the activity and scoring value. From the 3D modeling and binding interactions analysis, it was concluded that the driving forces for the potent α-amylase inhibitors to have similar binding poses as those found in acarbose are H-bonding, pi-pi stacking, and hydrophobic interactions (Rosas-Ramírez et al., 2018). All of which were observed in **1**, **2**, and **5** whereas the other analogs had a different binding mode that decreased their inhibitory activity against α-amylase. From the above analysis, it raised the question of why **1**, **2**, and **5** were more active among other analogs **3** and **4**. The xanthones analogs **1**, **2**, and **5** shared some important similarities such as inhibitory activity, binding pose, and the total score (Table 2, Fig. 5D). Therefore, it is worthy to have a deep analysis among them compared to acarbose and other analogs such as **3** and **4**. From the point of view of the 3D
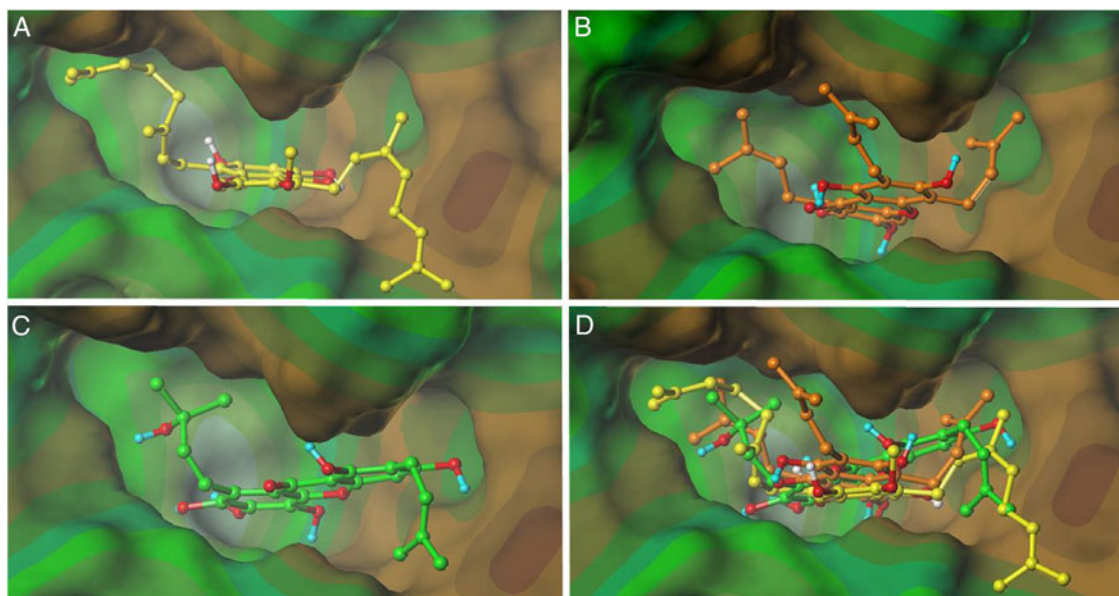
Fig. 5. 3D docked inhibitors in the active site. (A) **1** (yellow), (B) **3** (orange), (C) **2** (green), and (D) overlaid structures **1**, **2**, and **5**.

modeling, the docking results revealed that **1**, **2**, and **5** had shared the same binding region compared to acarbose whereas **3** and **4** did not share the same binding area. However, acarbose had two sugar moieties that preferred to interact with the polar regions of the enzyme *via* hydrogen bonding whereas the side chains of **1**, **2**, and **5** preferred the hydrophobic regions (Fig. 5A, B, and C). Specifically, the prenyl chain at C-2 of **5** interacted with the hydrophobic region that located next to the active site pocket whereas the long side chain at C-2 of **1** interacted with an extended hydrophobic region located outside the active site. However, **2** interacted with 3 different hydrophobic regions than **1** and **5**.

Structure-activity relationship (SAR)

Since all xanthones analogs are structurally related, it is noteworthy to address the structure-activity relationship (SAR) among them. The aliphatic substitutions on the xanthone structure at C-2, C-4, and C-8 positions are necessary to enhance the inhibitory activity as found in **1**, **2**, and **5**. The longer the side chains at C-4 and C-8, the greater the activity as observed in **1** (Ryu et al., 2011; Nguyen et al., 2017). The hydroxyl substitution at C-5 on the xanthone is very important; it formed H-bond with His-299 residue as in **5**. Losing or eliminating this particular group at this position resulted in decreasing the activity and therefore different binding interaction was illustrated as in **4**. Aliphatic side chain substitution at C-4 of the xanthone is recommended; it enhanced the inhibitory activity as revealed in **1** and **2**. The SAR studies herein are very important to elucidate the substantial substitution at different positions for the drug discovery process.

Conclusion

A new xanthone (**5**) and four known compounds (**1**–**4**) were isolated from *G. mangostana* pericarps. Their structures were assigned using different spectroscopic tools. Compounds **1**, **2**, and **5** showed potentially high α-amylase inhibitory activity compared with acarbose. The present study gave a scientific support to the use of *G. mangostana* pericarps in folklore medicine for treating diabetes. The antidiabetic activity of *G. mangostana* could be correlated to its xanthones metabolites. However more *in vivo*, *in vitro*, and clinical studies are required for further evaluation of its antidiabetic activities.

Authors' contributions

SRMI: manuscript submission, data acquisition, analysis, and interpretation of NMR data. GAM: plant collection, concept and design of the study, and supervision of the study. MTK: carrying out docking studies and writing their results. SA, HAH, and KZA: design of the study, interpretation of biological data, and sharing in writing the manuscript. All authors read and approved the final manuscript.

Conflicts of interest

The authors declare no conflicts of interest.

Appendix A. Supplementary data

Supplementary data associated with this article can be found, in the online version, at doi:10.1016/j.bjp.2019.02.005.

References

Abdallah, H.M., El-Bassossy, H., Mohamed, G.A., El-Halawany, A.M., Alshali, K.Z., Banjar, Z.M., 2016a. Phenolics from *Garcinia mangostana* inhibit advanced glycation endproducts formation: effect on amadori products, cross-linked structures and protein thiols. Molecules 21, 251–266.

Abdallah, H.M., El-Bassossy, H., Mohamed, G.A., El-Halawany, A.M., Alshali, K.Z., Banjar, Z.M., 2016b. Phenolics from *Garcinia mangostana* alleviate exaggerated vasoconstriction in metabolic syndrome through direct vasodilatation and nitric oxide generation. BMC Complement. Altern. Med. 16, http://dx.doi.org/10.1186/s12906-016-1340-1345.

Abdallah, H.M., El-Bassossy, H., Mohamed, G.A., El-Halawany, A.M., Alshali, K.Z., Banjar, Z.M., 2017. Mangostanaxanthones III and IV: advanced glycation endproduct inhibitors from the pericarp of *Garcinia mangostana*. J. Nat. Med. 71, 216–226.

Adnyana, K., Abuzaid, A.S., Iskandar, E.Y., Kurniati, N.F., 2016. Pancreatic lipase and α-amylase inhibitory potential of mangosteen (*Garcinia mangostana* linn.) pericarp extract. Int. J. Med. Res. Health Sci. 5, 23–28.

Barrett, M.L., Udani, J.K., 2011. A proprietary alpha-amylase inhibitor from white bean (*Phaseolus vulgaris*): a review of clinical studies on weight loss and glycemic control. Nutr. J. 10, 10–24.

Ghazali, S.A., Lian, G.E., Abd Ghani, K.D., 2010. Chemical constituent from roots of *Garcinia mangostana* (Linn.). Int. J. Chem. 2, 134–142.

Gyémánt, G.L., Nagy, K.V., Somsák, L., 2003. Inhibition of human salivary a-amylase by glucopyranosylidene-spiro-thiohydantoin. Biochem. Biophys. Res. Commun. 312, 334–339.

Ibrahim, S., Al-Ahdal, A., Khedr, A., Mohamed, G., 2017b. Antioxidant α-amylase inhibitors flavonoids from Iris germanica rhizomes. Rev. Bras. Farmacogn. 27, 170–174.

Ibrahim, S.R.M., Abdallah, H.M., El-Halawany, A.M., Nafady, A.M., Mohamed, G.A., 2018c. Mangostanaxanthone VIII, a new xanthone from Garcinia mangostana and its cytotoxic activity. Nat. Prod. Res., http://dx.doi.org/10.1080/14786419.2018.1446012.

Ibrahim, S.R.M., Abdallah, H.M., El-Halawany, A.M., Radwan, M.F., Shehata, I.A., Al-Harshany, E.M., Zayed, M.F., Mohamed, G.A., 2018d. Garcixanthones B and C, new xanthones from the pericarps of Garcinia mangostana and their cytotoxic activity. Phytochem. Lett. 25, 12–16.

Ibrahim, S.R.M., Mohamed, G.A., Abdel-Latif, M.M.M., El-Messery, S.M., Al-Musayeib, N.M., Shehata, I.A., 2015. Minutaside A, new α-amylase inhibitor flavonol glucoside from Tagetes minuta: antidiabetic, antioxidant, and molecular modeling studies. Starch/Stärke 67, 976–984.

Ibrahim, S.R.M., Mohamed, G.A., Al Haidari, R.A., El-Kholy, A.A., Zayed, M.F., Khayat, M.T., 2018e. Tagetnoic acid, a new lipoxygenase inhibitor peroxy fatty acid from Tagetes minuta growing in Saudi Arabia. Nat. Prod. Res., http://dx.doi.org/10.1080/14786419.2018.1488712.

Ibrahim, S.R.M., Mohamed, G.A., Elfaky, M.A., Al Haidari, R.A., Zayed, M.F., El-Kholy, A.A., Ross, S.A., 2018a. Garcixanthone A, a new cytotoxic xanthone from the pericarps of Garcinia mangostana. J. Asian Nat. Prod. Res., http://dx.doi.org/10.1080/10286020.2017.1423058.

Ibrahim, S.R.M., Mohamed, G.A., Elfaky, M.A., Zayed, M.F., El-Kholy, A.A., Abdel-mageed, O.H., Ross, S.A., 2018b. Mangostanaxanthone VII, a new cytotoxic xanthone from Garcinia mangostana. Z. Naturforsch. C 73, 185–189.

Ibrahim, S.R.M., Mohamed, G.A., Zayed, M.F., Ross, S.A., 2017a. 8-Hydroxyirilone 5-methyl ether and 8-hydroxyirilone, new antioxidant and α-amylase inhibitors isoflavonoids from Iris germanica rhizomes. Bioorg. Chem. 70, 192–198.

Jayaraj, S., Suresh, S., Kadeppagari, R.-K., 2013. Amylase inhibitors and their biomedical applications. Starch/Stärke 65, 535–542.

Loo, A.E., Huang, D., 2007. Assay-guided fractionation study of alpha-amylase inhibitors from Garcinia mangostana pericarp. J. Agric. Food Chem. 55, 9805–9810.

Mata, R., Cristians, S., Escandón-Rivera, S., Juárez-Reyes, K., Rivero-Cruz, I., 2013. Mexican antidiabetic herbs: valuable sources of inhibitors of α-glucosidases. J. Nat. Prod. 76, 468–483.

Mohamed, G.A., Alliuocide, G., 2008. A new flavonoid with potent α-amylase inhibitory activity from Allium cepa L. Arkivoc xi, 202–209.

Mohamed, G.A., Al-Abd, A.M., El-Halawany, A.M., Abdallah, H.M., Ibrahim, S.R.M., 2017. New xanthones and cytotoxic constituents from Garcinia mangostana fruit hulls against human hepatocellular, breast, and colorectal cancer cell lines. J. Ethnopharmacol. 198, 302–312.

Mohamed, G.A., Ibrahim, S.R.M., Shaaban, M.I.A., Ross, S.A., 2014. Mangostanaxanthones I and II, new xanthones from the pericarp of Garcinia mangostana. Fitoterapia 98, 215–221.

Nahoum, V., Roux, G., Anton, V., Rougé, P., Puigserver, A., Bischoff, H., Henrissat, B., Payan, F., 2000. Crystal structures of human pancreatic alpha-amylase in complex with carbohydrate and proteinaceous inhibitors. Biochem. J. 346 (Pt 1), 201–208.

Nguyen, N.K., Truong, X.A., Bui, T.Q., Bui, D.N., Nguyen, H.X., Tran, P.T., Nguyen, L.H.D., 2017. α-Glucosidase inhibitory xanthones from the roots of Garcinia fusca. Chem. Biodiv. 41, e1700232.

Qian, M., Spinelli, S., Driguez, H., Payan, F., 1997. Structure of a pancreatic alpha-amylase bound to a substrate analogue at 2.03 Å resolution. Protein Sci. 6, 2285–2296.

Rahimi, R., Nikfar, S., Larijani, B., Abdollahi, M., 2005. A review on the role of antioxidants in the management of diabetes and its complications. Biomed. Pharmacother. 59, 365–373.

Rosas-Ramírez, D., Escandòn-Rivera, S., Pereda-Miranda, R., 2018. Morning glory resin glycosides as α-glucosidase inhibitors: In vitro and in silico analysis. Phytochemistry 148, 39–47.

Ryu, H.W., Cho, J.K., Curtis-Long, M.J., Yuk, H.J., Kim, Y.S., Jung, S., Kim, Y.S., Lee, B.W., Park, K.H., 2011. α-Glucosidase inhibition and antihyperglycemic activity of prenylated xanthones from Garcinia mangostana. Phytochemistry 72, 2148–2154.

Sales, P.M., Souza, P.M., Simeoni, L.A., Magalhães, P.O., Silveira, D., 2012. α-Amylase inhibitors: a review of raw material and isolated compounds from plant source. J. Pharm. Pharmaceut. Sci. 15, 141–183.

Tucci, S.A., Boyland, E.J., Halford, J.C., 2010. The role of lipid and carbohydrate digestive enzyme inhibitors in the management of obesity: a review of current and emerging therapeutic agents. Diabetes Meta. Syndr. Obes. 3, 125–143.

Xu, Z., Huang, L., Chen, X.H., Zhu, X.F., Qian, X.J., Feng, G.K., Lan, W.J., Li, H.J., 2014. Cytotoxic prenylated xanthones from the pericarps of Garcinia mangostana. Molecules 19, 1820–1827.